ELSEVIER

Contents lists available at ScienceDirect

# Journal of Theoretical Biology

journal homepage: www.elsevier.com/locate/yjtbi



# Slowly activating outward membrane currents generate input-output sub-harmonic cross frequency coupling in neurons



Nirvik Sinha a,b, C.J. Heckman a,b,c, Yuan Yang a,b,d,e,\*

- a Northwestern Interdepartmental Neuroscience Program, Feinberg School of Medicine, Northwestern University, 320 E Superior Street, Morton 1-645, Chicago, IL 60611-3010, USA
- <sup>b</sup> Department of Physical Therapy and Human Movement Sciences, Feinberg School of Medicine, Northwestern University, 645 N. Michigan Ave., Suite 1100, Chicago, IL 60611, USA
- <sup>c</sup> Department of Physiology, Feinberg School of Medicine, Northwestern University, 310 E. Superior Street Morton 5-660, Chicago, IL 60611, USA
- <sup>d</sup> Stephenson School of Biomedical Engineering, University of Oklahoma, 4502 E. 41st St, Tulsa, OK 74135, USA <sup>e</sup> Laureate Institute for Brain Research, 6655 S Yale Ave, Tulsa, OK 74136, USA

#### ARTICLE INFO

## Article history: Received 1 April 2020 Revised 16 August 2020 Accepted 27 September 2020 Available online 3 October 2020

Keywords: Cross-frequency coupling Hodgkin-Huxley neuron Sub-harmonic coupling Slow potassium conductance

#### ABSTRACT

A major challenge in understanding spike-time dependent information encoding in the neural system is the non-linear firing response to inputs of the individual neurons. Hence, quantitative exploration of the putative mechanisms of this non-linear behavior is fundamental to formulating the theory of information transfer in the neural system. The objective of this simulation study was to evaluate and quantify the effect of slowly activating outward membrane current, on the non-linearity in the output of a onecompartment Hodgkin-Huxley styled neuron. To evaluate this effect, the peak conductance of the slow potassium channel ( $g_{K-slow}$ ) was varied from 0% to 200% of its normal value in steps of 33%. Both crossand iso-frequency coupling between the input and the output of the simulated neuron was computed using a generalized coherence measure, i.e., n:m coherence. With increasing g<sub>K-slow</sub>, the amount of subharmonic cross-frequency coupling, where the output frequencies (1-8 Hz) are lower than the input frequencies (15-35 Hz), increased progressively whereas no change in iso-frequency coupling was observed. Power spectral and phase-space analysis of the neuronal membrane voltage vs. slow potassium channel activation variable showed that the interaction of the slow channel dynamics with the fast membrane voltage dynamics generates the observed sub-harmonic coupling. This study provides quantitative insights into the role of an important membrane mechanism i.e. the slowly activating outward current in generating non-linearities in the output of a neuron.

© 2020 Elsevier Ltd. All rights reserved.

## 1. Introduction

In biological neurons, the action potential spike is the principal basis of information encoding and this property is remarkably preserved across different organisms and neuronal types. Besides the classical view of information being carried by modulation of the firing rates of neurons (Barlow et al., 1992), it is well recognized that spike timing is also used as the coding scheme in neural systems (Sejnowski, 1995; Fetz, 1997). The relative timing of firing has been shown to be an important computational property in neuronal assemblies for a diverse set of functions like distributed information processing in cortical microcircuits (Nessler et al., 2013), pattern recognition (Hu et al., 2013; Masquelier et al., 2009; Panzeri and Diamond, 2010; Tiesinga et al., 2008), encoding

E-mail address: yuan.yang-2@ou.edu (Y. Yang).

of behaviorally relevant information in the somatosensory and auditory systems (Saal et al., 2016) and Hebbian learning (Caporale and Dan, 2008). In the terms of the motor system, although rate coding plays a predominant role due to different recruitment thresholds of motor units (Enoka and Duchateau, 2017), millisecond-scale variations in the timing of spikes have been shown to play a crucial role in predicting and causally controlling behavior (Srivastava et al., 2017). Recent work has shown that spike timing codes are ubiquitous, consistent, and essential for all motor coordination (Putney et al., 2019).

A major factor that influences the temporal activity of individual neurons is the non-linearity of spike train output in response to a time varying input they receive from a multitude of synapses. Different types of neuron have their own repertoire of ion channels that is responsible for their characteristic non-linear firing patterns and also their unique neurocomputational properties (Jeong, et al., 2012). For example, activation of the L-type calcium channels in nigral dopaminergic neurons results in intrinsic

<sup>\*</sup> Corresponding author at: Stephenson School of Biomedical Engineering, University of Oklahoma, 4502 E. 41st St, Tulsa, OK 74135, USA.

bursting behavior which has been shown to exhibit lowdimensional determinism and likely encodes meaningful information in the awake state (Jeong, et al., 2012). Persistent inward currents mediated by their voltage-gated sodium and calcium channels are an important source of non-linear behavior of spinal motoneurons and is instrumental for generating the sustained force outputs required for postural control (Hounsgaard et al., 1988). Indeed, modulation of these channels by descending monoaminergic inputs acts as a gain control mechanism for the somatic motor system (Cameron et al., 1980; Wei et al., 2014; Binder et al., 2020). Fast kinetics of the post-hyperpolarizing potassium channel is responsible for maintaining the firing state of cortical interneurons near the Andronov-Hopf bifurcation point thereby making them ideal candidates for processing information restricted to specific oscillatory phases (Stiefel et al., 2013). Thus, quantitative exploration of the role of individual ion channels in the modulation of the output behavior of neurons is essential for understanding the general principles of information encoding employed by the neural system.

The nonlinear relation between the time-varying input to the neuron and its spike train output, mediated by its component ion channels, can generate various types of input-output interactions such as harmonic, subharmonic and/or intermodulation coupling (Roberts and Robinson, 2012). Since a linear system can only generate *iso*-frequency coupling (quantified by linear coherence or cross-correlation) between an input and the output, nonlinearity of a system can be easily detected in the frequency domain by measuring the input-output interactions across different frequencies (McGee et al., 2005; Shils et al., 1996; Victor and Shapley, 1980; Miles et al., 2007).

Spike-frequency adaptation (SFA) i.e. the slowing of neuronal firing rate in response to a constant stimulus is a ubiquitous neuronal process that has a prominent effect on its dynamics (Laughlin, 1989). Ionic mediators of SFA are diverse and include: (i) M-type currents generated by voltage-dependent, high threshold potassium channels (Brown and Adams, 1980), (ii) post-hyperpolarization-type currents mediated by calciumdependent potassium channels (Madison and Nicoll, 1984), (iii) slow recovery from inactivation of the fast sodium channel (Fleidervish et al., 1996), (iv) sodium-sensitive potassium currents (Bhattacharjee and Kaczmarek, 2005) and, (v) calciumsensitive chloride current (De Castro et al., 1997). Each of these has been observed in a variety of systems and is involved in different neurocomputational functions (Peron and Gabbiani, 2009). However, all the mediators have the same underlying mechanism of membrane hyperpolarization operating on a relatively slower time scale as compared to those membrane mechanisms that generate the action potential (i.e. the fast sodium and potassium currents).

The objective of this simulation study was to evaluate and quantify the effect of this slow membrane hyperpolarization mechanism (using the M-type current which mediates SFA induced spike-time modulation) on the non-linearity in the output of a one-compartment Hodgkin-Huxley styled neuron (spike-trains convolved with an EPSP) driven by a time-varying input current. We hypothesized that the slow time scale of this mechanism generates increased subharmonic coupling between the input and the output. To test our hypothesis, we systematically varied the peak conductance of the M-type potassium channel of our model which resembles the strength of its coupling with the membrane voltage. We showed how changes in this parameter produce systematic changes in the non-linear input-output coupling of the model neuron using a generalized coherence measure i.e. n:m coherence (Yang et al., 2016). Furthermore, we explored the underlying mechanisms of the observed changes in non-linearity using power spectral and phase space analysis.

## 2. Methods

## 2.1. Neuron model

A one-compartment Hodgkin-Huxley styled neuron model was used for our simulations. The minimalist model incorporated the following ionic currents (with the corresponding channel conductances): fast sodium ( $I_{Na}$  with maximal conductance  $g_{Na}$ ) (Traub et al., 1991), delayed-rectifier potassium ( $I_K$  with maximal conductance  $g_K$ ) (Traub et al., 1991), slow non-inactivating M-type potassium ( $I_{K-slow}$  with maximal conductance  $g_{K-slow}$ ) (Yamada et al., 1989), and leakage ( $I_L$  with constant conductance  $g_L$ ) currents:

$$I_{Na} = g_{Na} \times m_{Na}^3 \times h_{Na} \times (V - E_{Na}) \tag{1}$$

$$I_K = g_K \times m_K^4 \times (V - E_K) \tag{2}$$

$$I_{K-slow} = g_{K-slow} \times m_{K-slow} \times (V - E_K)$$
 (3)

$$I_{L} = g_{I} \times (V - E_{L}) \tag{4}$$

where V is the membrane potential of the neuron.  $E_{Na}$ ,  $E_K$ , and  $E_L$  are the reversal potentials for sodium, potassium, leakage currents, respectively. The voltage gated sodium and fast potassium channel is responsible for the spiking behavior while the M-channel serves as an abstraction for the slowly activating outward membrane current that mediates spike-frequency adaptation. The variables m and h (with subscripts indicating ionic channels) represent the activation and inactivation variables of the corresponding ionic channels, as described by the following differential equations:

$$\tau_{m,i}(V)\frac{d}{dt}m_i = m_{\infty,i}(V) - m_i \tag{5}$$

$$\tau_{h,i}(V)\frac{d}{dt}h_i = h_{\infty,i}(V) - h_i \tag{6}$$

where i indicates the name of the channel,  $m_{\infty,i}(V)$  and  $h_{\infty,i}(V)$  represent the voltage-dependent steady-state activation and inactivation, and  $\tau_{m,i}(V)$  and  $\tau_{h,i}(V)$  are the corresponding time constants. The steady-state activation and the time constant are given by:

$$m_{\infty,i}(V) = \frac{\alpha_{m,i}(V)}{\alpha_{m,i}(V) + \beta_{m,i}(V)}$$
(7)

$$\tau_{m,i}(V) = \frac{1}{\alpha_{m,i}(V) + \beta_{m,i}(V)}$$
(8)

and similarly, for h.  $\alpha_i$  and  $\beta_i$  are the forward and backward rates of the first order gating kinetics of the  $i^{th}$  ion channel between the closed (C) and open (O) states:

 $\alpha_i(V)$ 

$$C \leftrightarrow 0$$
 (9)

 $\beta_i(V)$ 

The membrane potential of the neuron (*V*) was computed from the following first-order differential equation:

$$C\frac{dV}{dt} = -I_{Na} - I_K - I_{K-slow} - I_L + I_{inj}$$
(10)

where C is the membrane capacitance (1  $\mu$ F/cm<sup>2</sup>),  $I_{inj}$  is the time-varying input as described below and t is time. The parameters of this model are based on experimentally fitted values of cortical interneurons (Pospischil et al., 2008) (see *Appendix* and Table 1 for details of these parameters and values of all constants).

## 2.2. Input signal

The input to the neuron was designed as a beta-band signal  $(15\text{--}35\text{ Hz}, 1\text{ Hz} \text{ resolution}, \text{sum of sinusoids with uniform random phase } \in [0, 2\pi])$  with power values of each frequency being drawn from a Gaussian profile ( $\mu$  = 25 Hz,  $\sigma$  = 3.3 Hz), mimicking the cortical oscillations observed experimentally during the awake state (Pfurtscheller and Da Silva, 1999). Subsequently we added a membrane noise to this signal (see Fig. 1). The membrane noise represents stochastic membrane perturbations of biological neurons (Faisal et al., 2008) and we modeled them as a zero-mean Wiener process (Maltenfort et al., 1998).

## 2.3. Simulations

To test the effect of slow outward membrane current, we varied the peak conductance  $g_{K\text{-}slow}$  of the M-type slow potassium channel, which controls the amount of slow hyperpolarizing current in our model, from 0.0 mS/cm² (i.e. no M-channel) to 0.18 mS/cm² in steps of 0.03 mS/cm². These values covered the entire range of experimentally fitted values of  $g_{K\text{-}slow}$  for different types of cortical interneurons (Pospischil et al., 2008). Since the output spike train of a single neuron (given an input with SNR -3.3 dB) has very low power in the input signal frequencies, the coherence estimation between its input and output will not be significant (unless it has an unnaturally high firing rate of the order of kHz, see for example Fig. 5B of (Negro and Farina, 2011). Thus, to obtain signif-

icant input-output coherence we needed to sum together the output across several simulation runs. For this purpose, if we fixed the firing rate at any particular value, it would have been difficult to demonstrate the generalizability of our results across different firing rates. Therefore, we decided to adopt a biologically plausible firing rate range of 5-50 spikes/s across 30 simulation runs. If we keep all other parameters constant, increasing  $g_{K-slow}$  decreases the firing rate of the neuron and vice versa. Hence, we adjusted the recruitment threshold of the neuron (by tuning the equilibrium potential  $E_L$  (Rybak et al., 2006/12/01/2006) so that for different values of  $g_{K-slow}$  we have the same firing rate. For each value of  $g_{K-slow}$ , our code first optimizes the range of  $E_L$  values needed to produce firing rates in the range of  $\approx$ 5–50 spikes/s across the 30 simulations. In other words, for each value of  $g_{K-slow}$  we have a particular range of optimized  $E_l$  values so that the range of the resultant firing rates is the same. One issue with artificially manipulating the  $E_{l}$  in this way could be that even though the range of the resultant firing rates remain the same, the distribution is altered because of a non-linear relation between the two. Fortunately, we found this not to be the case. Using the optimized  $E_L$  values, for each  $g_{K-slow}$ , the distribution of the firing rates was found to be the same (see Fig. 2). All simulations were performed in Julia using the stiff stochastic differential equation solver SkenCarp of the DifferentialEquations package (Rackauckas and Nie, 2017). Each run of the simulation was conducted at a sampling rate of 100 kHz for 200 s. The 1st 10 s were thereafter discarded to consider only the steady-state behavior of the neuron. The resulting

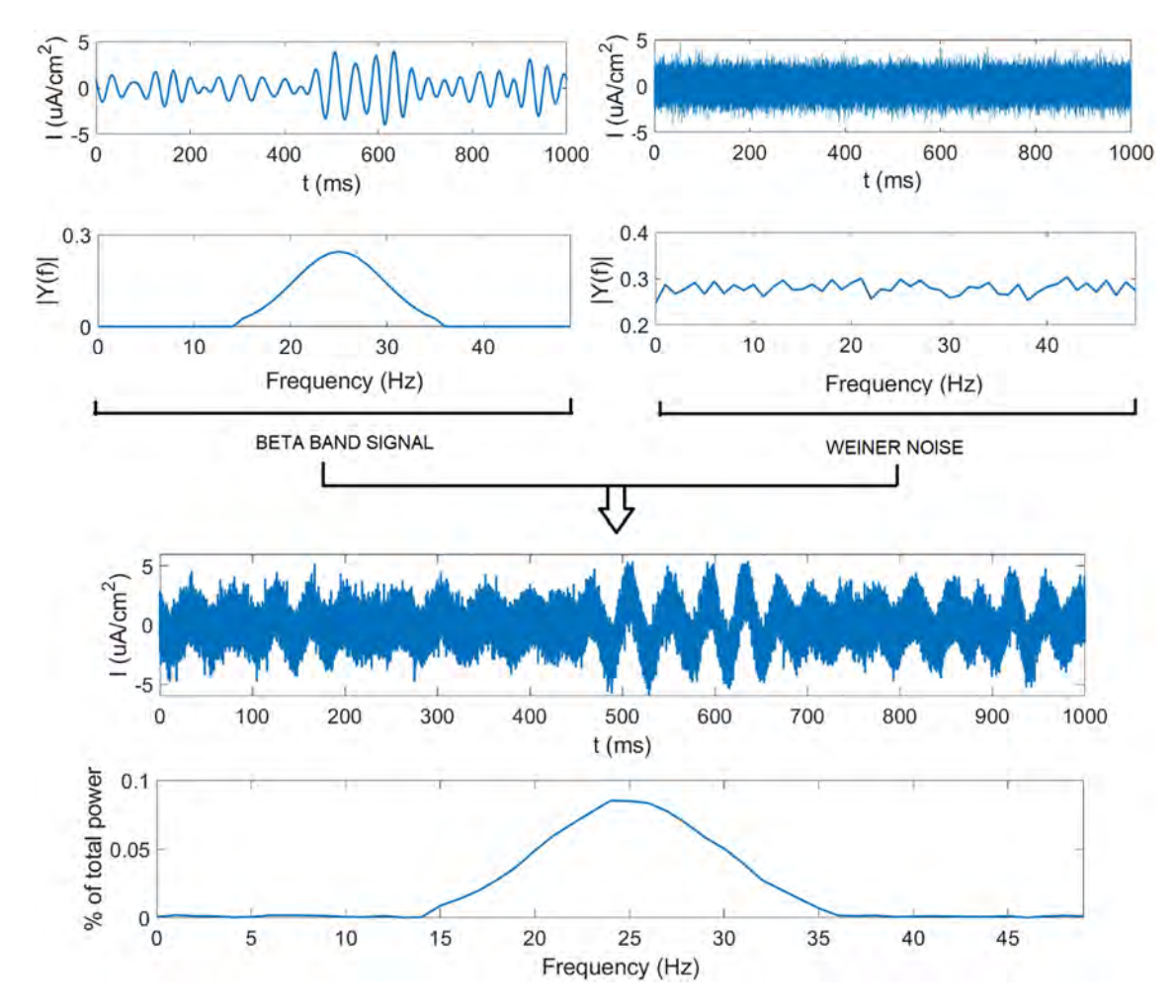
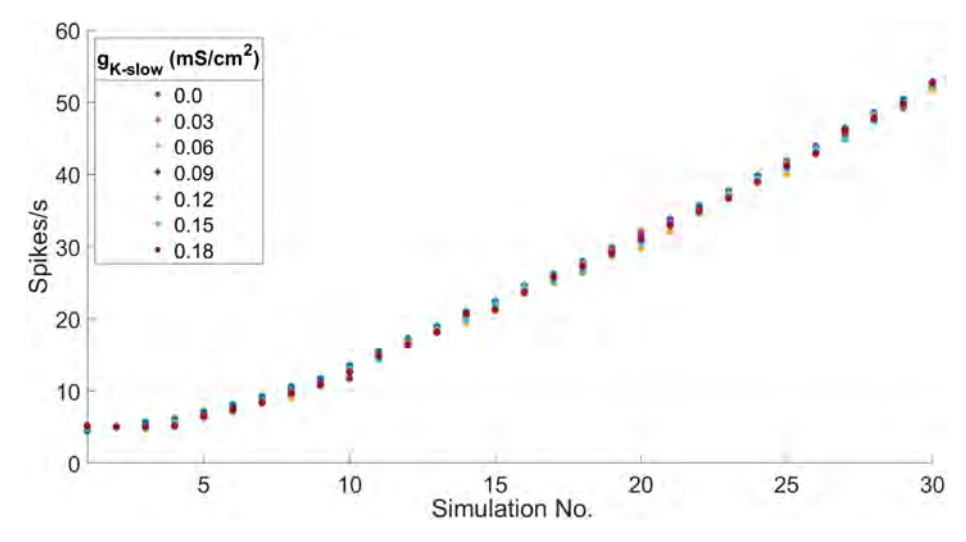


Fig. 1. Input design. The input to the neuron model was designed as a combination of beta-band (15–35 Hz) Gaussian signal with added membrane noise. The signal-to-noise ratio was -3.3 dB.



**Fig. 2.** Distribution of firing rates. For every level of peak slow potassium conductance ( $g_{K-slow}$ ), a set of 30 simulations were conducted by varying the leakage potential  $E_L$  of the neuron to get the same distribution of firing rates in each case.

data was sufficient for a robust neural coupling analysis (Hagihira et al., 2001).

## 2.4. Data analysis

The data of each 190 s simulation were divided into 1 s non-overlapping epochs and the spike trains of each epoch were obtained in 1 ms bins. Subsequently, to convert the output spike trains to continuous signals, they were convolved with a normalized alpha function (time constant of 5 ms) to construct a continuous signal resembling a train of excitatory post-synaptic potentials (EPSP) (Dayan and Abbott, 2005). Fig. 3 shows a sample trace of the membrane voltage and the corresponding EPSP. The EPSP signals from the set of 30 simulations per step of  $g_{K-slow}$  were summed together to constitute the output signal for subsequent analysis.

We used our recently developed generalized coherence measure, i.e., n:m coherence (NMC) (Nikias and Mendel, 1993), to assess cross- and *iso*-frequency coupling between the simulated input and the output signals. The n:m coherence is a straightforward extension of the linear coherence based on high-order statistics (Yang et al., 2016) for distinguishably determining cross- and *iso*-frequency coupling between signals. Thus, the *iso*-frequency coupling obtained by this method is comparable to linear coherence.

Let X(f), Y(f) be the Fourier Transform of two time series (e.g. the input and output signals). The NMC between them is defined as:

$$NMC(f_X, f_Y) = \frac{|S_{XY}(f_X, f_Y)|}{\sqrt{S_X^n(f_X)S_Y^m(f_Y)}}$$
(11)

for assessing cross-frequency  $(f_X \neq f_Y)$  and iso-frequency  $(f_X = f_Y)$  coupling between signals, wherem/n is the simple whole number ratio of  $f_X/f_Y$  (e.g. if  $f_X = 8$ ,  $f_Y = 16$  then m = 1, n = 2) and

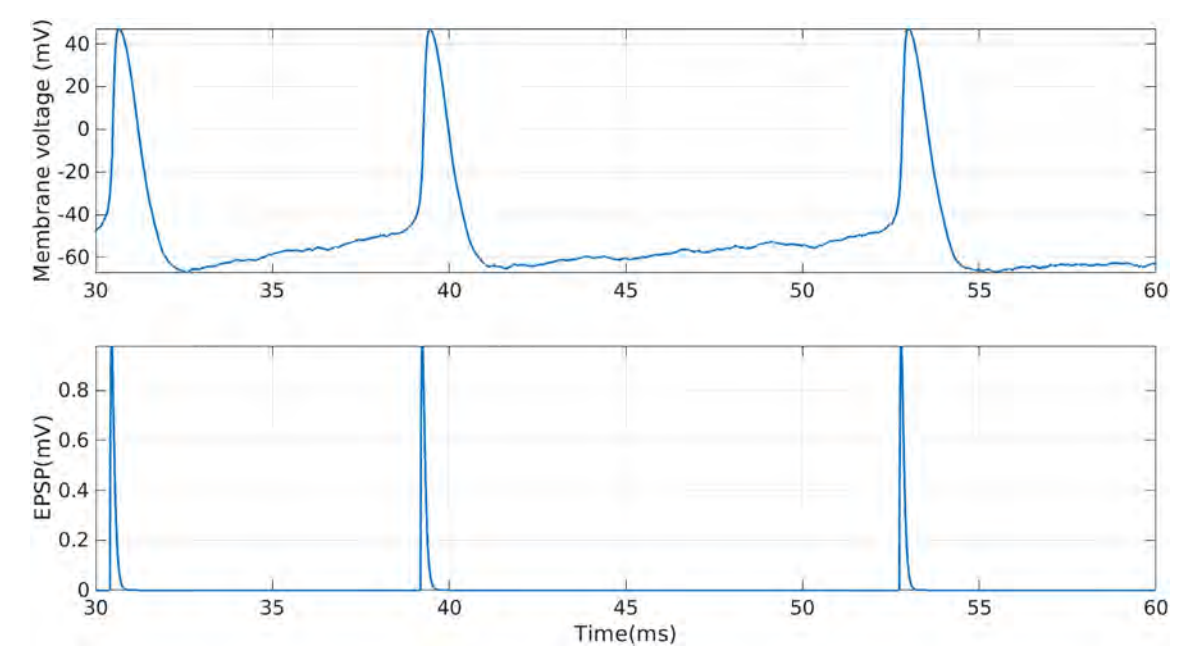


**Fig. 3.** Sample trace of the membrane voltage of the simulated neuron and its corresponding EPSP signal: The EPSP signal was obtained by convolving the spike train with an alpha-function. [Neuron parameters: peak slow potassium conductance,  $g_{K-slow} = 0.09 \text{ mS/cm}^2$ , epoch-averaged firing rate = 50 spikes/s, epoch no. = 100,  $E_L = 34.6 \text{mV}$ ]

$$S_{XY}(f_X, f_Y) = \langle X^n(f_X)(Y^m(f_Y))^* \rangle,$$
 (12)

$$S_{x}^{n}(f_{x}) = \langle X^{n}(f_{x})(X^{n}(f_{x}))^{*} \rangle \tag{13}$$

where <-> represents the averaging over epochs and

$$X^{n} = \underbrace{X(f_{X}), X(f_{X}), \dots, X(f_{X})}_{n}$$
(14)

The NMC reflects the strength of iso- or cross-frequency coupling between signals. When  $f_X = f_Y$ , we have m = n = 1, then the NMC is equivalent to the classical (linear) coherence for *iso*-frequency coupling (Yang et al., 2015). When  $f_X \neq f_Y$ ; then the NMC indicates the non-linear coupling between signals across different frequency components (i.e. cross-frequency coupling) (De Hemptinne, 2013). Thus, the n:m mapping can generate both integer and non-integer harmonic (m > n) and sub-harmonic (m < n) coupling between the input and the output in the frequency domain (Nikias and Mendel, 1993). As a generalized coherence method, the NMC is a metric indicating cross-frequency coherence between signals, which is different from other cross-frequency coupling methods such as the phase-amplitude coupling (Yang et al., 2016) reflecting how a low-frequency phase modulates a high-frequency amplitude.

According to Cauchy-Schwarz-inequality, we have:

$$|\langle X^{n}9(f_{X})(Y^{m}(f_{Y}))*>| \leq (\langle |X^{n}(f_{X})|^{2}>)(\langle |Y^{m}(f_{Y})|^{2}>)$$
 (15)

Thus, the NMC is bounded by 0 and 1, where 1 indicates that two signals are perfectly coupled at the tested frequency pair ( $f_X$ ,  $f_{\rm Y}$ ). As the NMC values are computed by comparing different frequency pairs between signals, the significant threshold was adapted with a Bonferroni correction to control the type I error (family-wise error rate: 0.05) (Nikias and Mendel, 1993). There are 2100 frequency pairs that were included for Bonferroni corrections (15–35 Hz in the input  $\times$  1–100 Hz in the output). More details of the NMC method is available in (Nikias and Mendel, 1993). Since the input to our neuron model has a noise component, each coupling analysis was repeated 100 times, each time with a different realization of the Wiener noise added to the beta-band input in the same signal-to-noise ratio as the original input (i.e. -3.3 dB, see Simulations and Fig. 1). For each level of  $g_{K-slow}$ , the total amount of iso-frequency coupling (IFC), harmonic coupling (HC) and sub-harmonic coupling (SHC) between the beta-band input and the neuron output was computed using n:m coherence. Thus, there were 100 values of IFC, HC and SHC for each  $g_{K-slow}$ . All the data groups for the following analysis were first tested for homogeneity of variances using Bartlett's test and normality using Anderson-Darling test. To test for the effect of  $g_{K-slow}$  on IFC, HC, and SHC, we used one-way ANOVA followed by Tukey's post hoc test. Where the condition of homogeneity of variances was not met, we used Welch's ANOVA followed by Games-Howell's post hoc test. Likewise, where the condition of normality was not met, we used the non-parametric Kruskal-Wallis followed by Dunn-Sidák post hoc test. A significance level of 0.05 was used for all the statistical tests.

# 3. Results

The n:m coherence was analyzed between the time-varying input and the EPSP output of the neuron for every step of  $g_{K-slow}$ . Both iso- and cross-frequency coupling (IFC and CFC) was detected between the input and the output (see Fig. 4). Moreover, the detected CFC included both harmonic and sub-harmonic coupling. Using Kruskal-Wallis test, we found no significant effect of the peak M-channel conductance ( $g_{K-slow}$ ) on the amount of IFC [F (6,693) = 0.97, p = 0.98] (see Fig. 5). Using one-way ANOVA, we

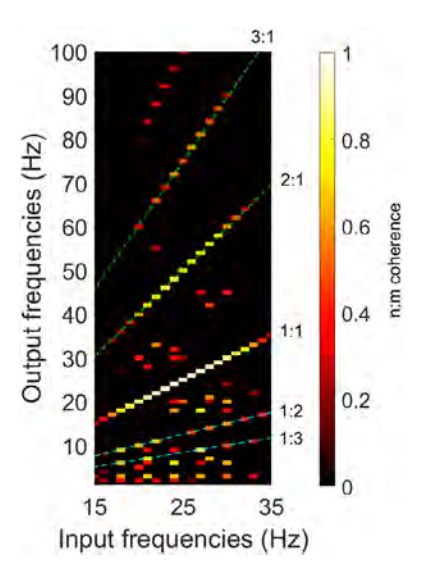


**Fig. 4.** Neural coupling between the beta-band (15–25 Hz) input and the output of the neuron (peak slow potassium conductance,  $g_{K-slow} = 0.09 \text{mS/cm}^2$ ). Both *iso*-frequency (1:1) and cross-frequency coupling (m:n, where  $m \neq n$ ) was detected. Cross frequency coupling includes both integer and non-integer harmonic (m > n) and sub-harmonic (m < n) coupling. Thus, harmonic coupling includes all the coupling values above the *iso*-frequency (1:1) coupling. Integer harmonic coupling (n = 1 and m > n) is shown by green-dashed lines (2:1 and 3:1). Integer sub-harmonic coupling ((m = 1 and n > m) is shown by blue-dashed lines (1:2 and 1:3). Non-integer harmonic (m > n and m,  $n \neq 1$ ) and sub-harmonic (n > m and m,  $n \neq 1$ ) coupling is also visible. (For interpretation of the references to colour in this figure legend, the reader is referred to the web version of this article.)

found that  $g_{K\text{-}slow}$  had a significant effect on both harmonic [F (6,693) = 52.36, p < 0.001] and sub-harmonic [F(6,693) = 214.09, p < 0.001] CFC. Using the Tukey's criterion for post hoc comparisons, we found that while there was a slight decrease in harmonic CFC, sub-harmonic coupling increased progressively with increasing  $g_{K\text{-}slow}$  from 0.0 to  $0.12\text{mS/cm}^2$  after which there was saturation (see Fig. 6). This shows that the strength of the slow potassium conductance has a strong positive correlation predominantly with the subharmonic component of the cross-frequency coupling wherein frequencies (15–35 Hz) in the time-varying injected current are phase-amplitude coupled with lower frequencies (<15 Hz) in the EPSP output of the neuron consistently across multiple epochs.

To further investigate how subharmonic input–output coupling is generated, we examined the power spectrum of the neuron outputs. The power spectrum showed a progressive increase in the amplitude of low-frequencies (predominantly in 1–4 Hz) with an increase of  $g_{K\text{-}slow}$  while the amplitude of higher frequencies (>8 Hz) remained constant (see Figs. 7 and 8). Thus, with the increase of  $g_{K\text{-}slow}$ , there is  $de\ novo$  increase in power of the low-frequency oscillations in the EPSP output of the neuron. Since the power of the input frequencies remain constant, selective increase in power of the low-frequencies in the output, results in progressive increase of subharmonic cross-frequency coupling, as shown by the n:m coherence measure.

Finally, we wanted to definitively implicate the slow potassium channel as the sole source of the increase in low-frequency oscillations in the neuronal output. To do this, we first examined the temporal profile and the corresponding power spectrum of the activity of the gating variables of the three ion channels in our model i.e. sodium, delayed rectifier potassium and the M-channel (see Fig. 9a and b). For the same time-varying input, the temporal dynamics of the slow potassium channel activation gate showed significantly higher power in the low-frequencies (1–4 Hz) as compared to the gating variables of the other ion channels. So, the

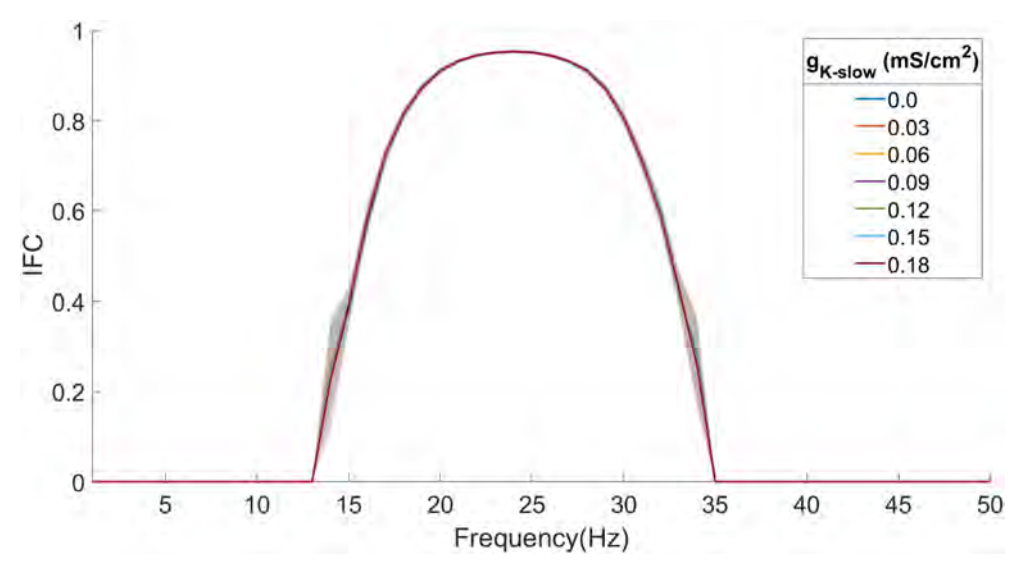


**Fig. 5.** Linear (iso-frequency) coupling between the beta-band (15–35 Hz) input and the output of the neuron for all levels of  $g_{K-slow}$ . No changes were seen in linear coupling with increasing levels of peak slow potassium conductance,  $g_{K-slow}$  (p = 0.986). The shaded area indicates  $\pm$  SEM.

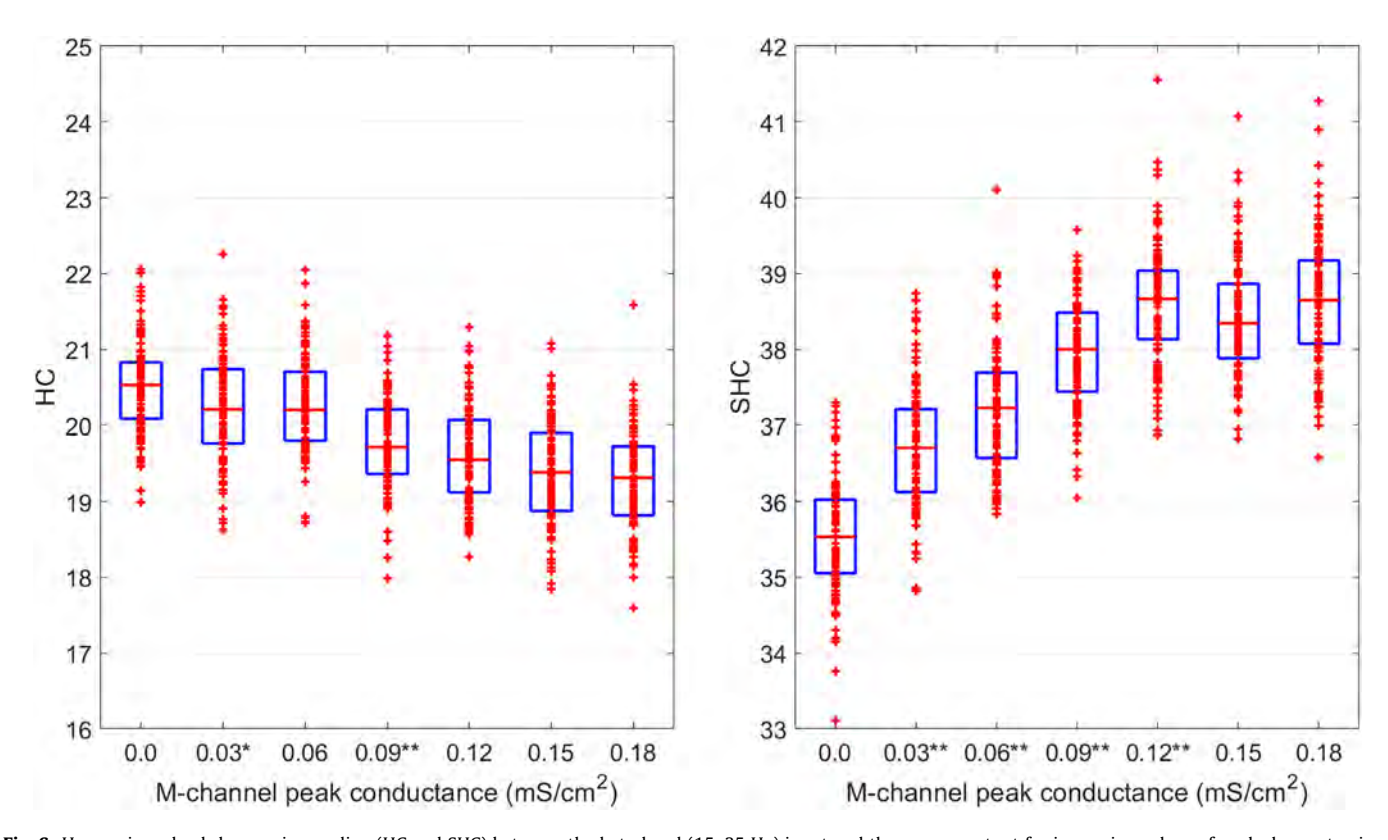


**Fig. 6.** Harmonic and sub-harmonic coupling (HC and SHC) between the beta-band (15–35 Hz) input and the neuron output for increasing values of peak slow potassium conductance  $g_{K-slow}$ . Each coupling analysis was repeated 100 times, each time with a different realization of the Wiener noise added to the beta-band input in the same signal-to-noise ratio as the original input (i.e. -3.3 dB, see Simulations and Fig. 1). For each level of  $g_{K-slow}$ , the total amount of *iso*-frequency coupling (IFC), harmonic coupling (HC) and sub-harmonic coupling (SHC) between the beta-band input and the summed EPSP signals from the set of 30 simulations was computed using n:m coherence. Thus, there were 100 values of IFC, HC and SHC for each level of  $g_{K-slow}$ . On each box, the central mark indicates the median, and the bottom and top edges of the box indicate the 25th and 75th percentiles, respectively. Individual datapoints are plotted using the '+' symbol. Asterisks in superscript of the n<sup>th</sup> level indicate a significant change of the value from the previous (n-1)<sup>th</sup> level. (Tukey's *post hoc* test, \*\* p < 0.001, \* p < 0.005).

question that arises from this observation is how do the low-frequency oscillations in the activity of the slow potassium gate percolate to the neuronal membrane dynamics? To investigate this, we examined the dynamics of the neuron on a phase plane. The state of the neuron at any time-point corresponds to a point on the phase plane. Since our neuron model is five-dimensional

(comprising of the neuronal output, activation, and inactivation sodium gates and one activation gate each for the fast and slow potassium currents), the complete phase plane for this model would be a five-dimensional hyperplane. However, as observed earlier, because of the slow time-scale of operation, low frequencies are predominantly present in the activation variable  $m_{K-slow}$ 

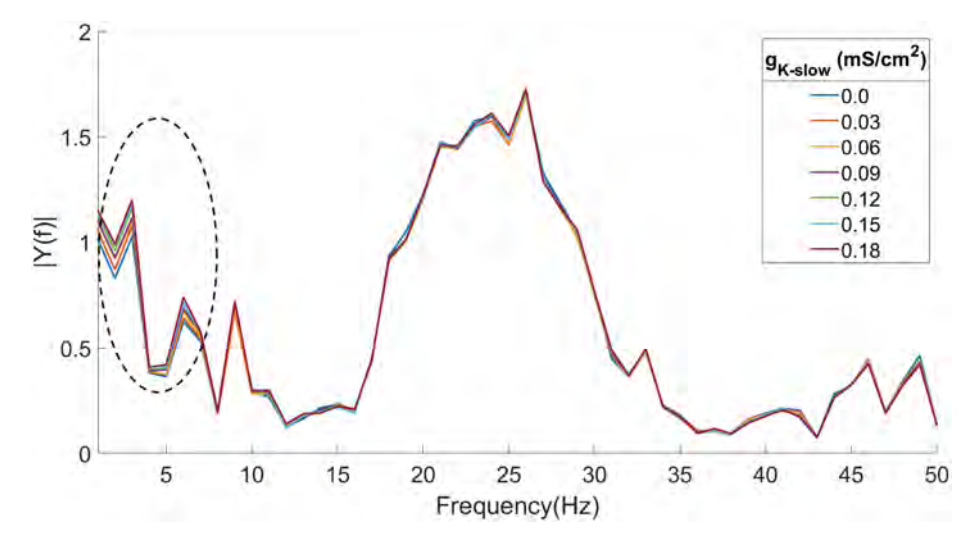


**Fig. 7.** Power spectrum of the neuron output for increasing levels of peak slow potassium conductance  $g_{K-slow}$ . For each level of  $g_{K-slow}$ , the summed EPSP signals from 30 runs of 190 s simulations were divided into 1 s non-overlapping epochs and the power spectrum was computed using the fast Fourier transform at 1 Hz resolution. With increasing levels of  $g_{K-slow}$ , there is a progressive increase in power in the low frequencies (<8 Hz) whereas there is no change in power in the higher frequencies.

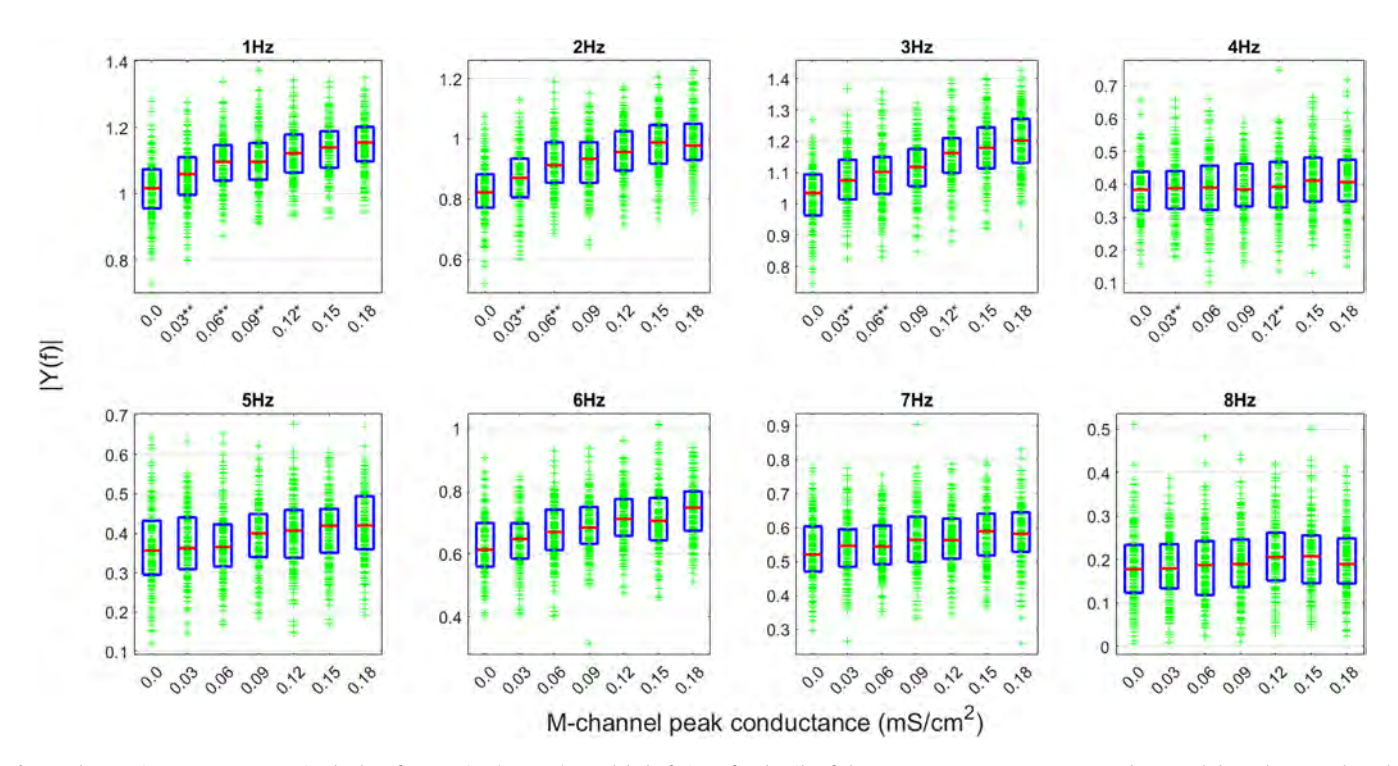
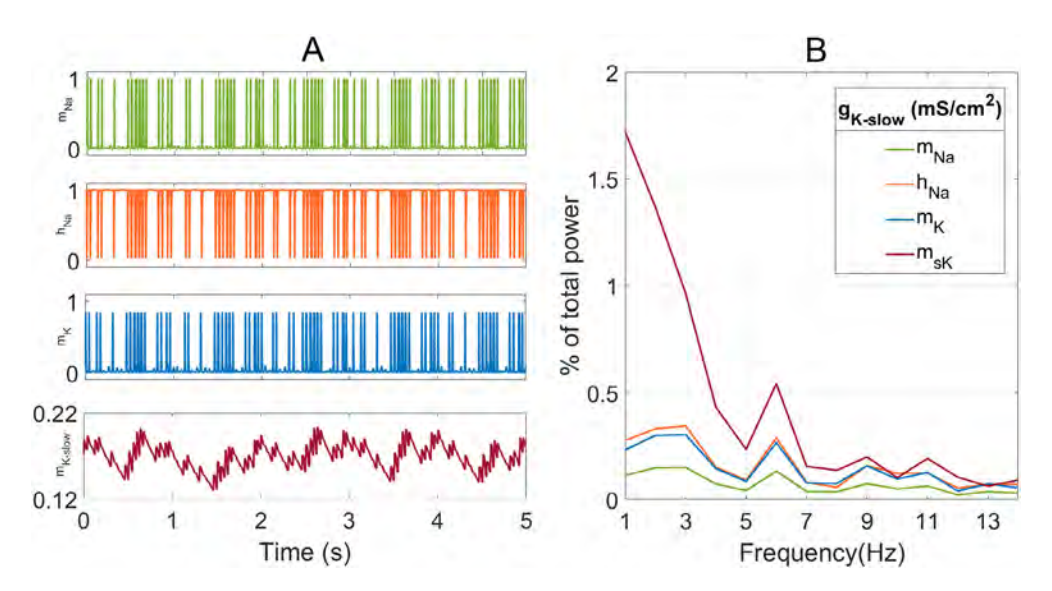


Fig. 8. Changes in power spectrum in the low frequencies (1–8 Hz). See label of Fig. 7 for details of the power spectrum was computed. On each box, the central mark indicates the median power value, and the bottom and top edges of the box indicate the 25th and 75th percentiles, respectively. Individual epoch-wise power values are plotted using the '+' symbol. There was progressive increase in power in the lower frequencies, especially in 1 Hz (Welch's ANOVA: F(5,528.53) = 159.50, p < 0.001), 2 Hz (one way ANOVA: F(5,1134) = 54.51, p < 0.001), 3 Hz (one way ANOVA: F(5,1134) = 70.73, p < 0.001) and 4 Hz (one way ANOVA: F(5,1134) = 67.0415, p < 0.001). Asterisks in superscript of the P(5,1134) = 10.001 in the previous level. (Games-Howell/Tukey's post hoc test, \*\* P < 0.001, \* P < 0.005).

of the M-channel. Hence, we restricted the phase-plane analysis to the neuronal output (i.e. the pooled EPSP) and  $m_{K-slow}$  because these are the most pertinent state variables for examining the emergence of observed sub-harmonic input-output coupling. We conducted the phase-plane analysis for low frequencies by band-pass filtering the pooled EPSP and  $m_{K-slow}$  for each level of  $g_{K-slow}$  (1-4 Hz cut-off, 2nd order Butterworth filter, see Fig. 10). Due to the presence of noise in the input, the trajectory of the orbits exhibited jitter. Despite the jitter, with increasing  $g_{K-slow}$  the trajectory progres-

sively converged to a limit cycle attractor in a tighter fashion. This result shows that with increasing  $g_{K-slow}$  there was increased low-frequency phase-locking between neuronal output and  $m_{K-slow}$  across epochs. Furthermore, to quantify the strength of phase locking, we measured the phase-locking value (PLV) between the slow potassium channel activation gate and the neuronal output across all the epochs for the different values of  $g_{K-slow}$  using a generalized phase coupling measure called multi-spectral phase coherence (MSPC) (Benda and Herz, 2003). For any two time series x(t) and



**Fig. 9.** Time profile of activation of the ion channel gating variables (peak slow potassium conductance,  $g_{K-\text{slow}} = 0.09\text{mS/cm}^2$ ). The sodium activation and inactivation gates ( $m_{Na}$  and the fast potassium activation gate ( $m_K$ ) have dominant fast kinetics while the slow potassium gate ( $m_{K-\text{slow}}$ ) has dominant slow kinetics. The traces show the activity of the gates with the same input driving the neuron in its steady-state as described in Input signal in Methods. B: Power spectrum of the activity of the channel gates in A. The slow potassium activation gate shows a larger amount of low-frequency activity ( $m_{K-\text{slow}}$ ) as compared to the other gating variables.

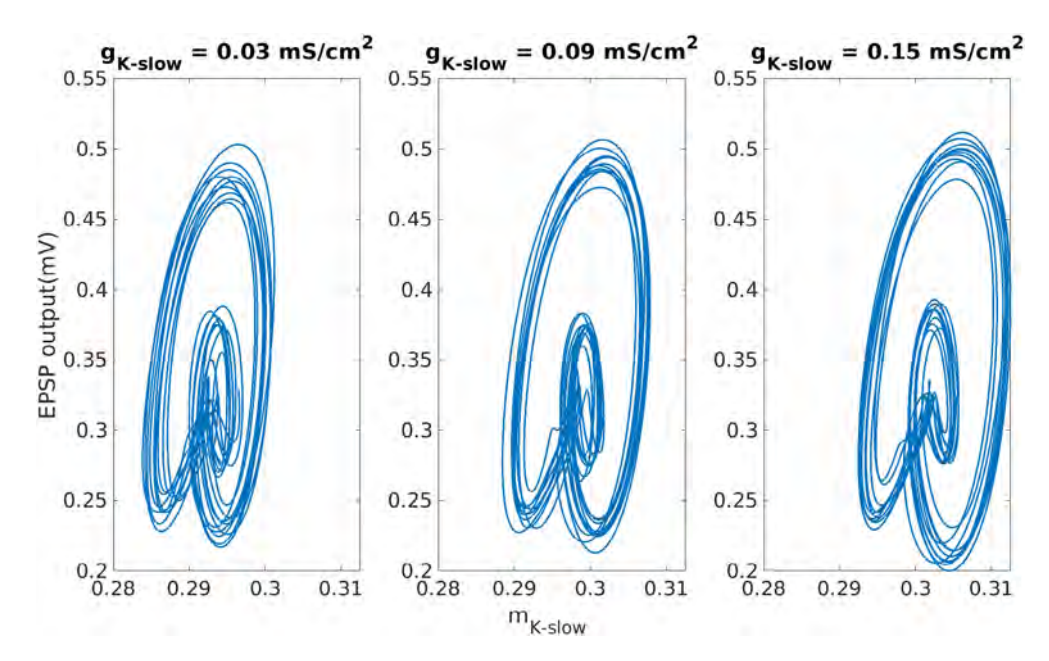


**Fig. 10.** Phase-portrait of the pooled activity of the slow potassium activation variable  $(m_{K-slow})$  vs. neuronal output (EPSP). The signals were band-pass filtered (2nd order Butterworth, 1–4 Hz cut-off) to examine the degree of phase-locking at low frequencies with increasing peak slow potassium conductance  $(g_{K-slow})$ . The phase portrait was constructed using data from 10 consecutive 1 s epochs in the steady-state condition (epochs no. 101 to 110).

y(t) with K epochs (i.e. trials), let X(f) and Y(f) be their Fourier transforms. The multi-spectral MSPC at the  $d^{th}$  order is defined as the magnitude (denoted as  $\psi$ ) of the complex measure called multi-spectral phase coherency (denoted as  $\Psi$ ):  $\psi = |\Psi|$ , for quantifying the  $d^{th}$  phase coupling. The multi-spectral phase coherency  $\Psi$  is defined by:

$$\Psi_{XY}(f_1, f_2, \dots f_R; a_1, a_2, \dots a_R)_d = \frac{1}{K} \sum_{k=1}^K e^{j \sum_{r=1}^R (a_r \Phi x_k(f_r) - \Phi y_k(f_\Sigma))}$$
(16)

where  $f_{\Sigma}$  is an output frequency of Y(f) as defined before,  $f_1, f_2, \dots f_R$  are the input frequencies of X(f),  $\Phi x_k(f_r)$  is the phase of

 $X(f_r)$ at the  $k^{th}$  epoch,  $a_1, a_2, \cdots a_R$  are the weights of input frequencies to corresponding output frequency  $f_{\Sigma}$  and,

$$\sum_{r=1}^{R} |a_r| = d \tag{17}$$

Details about the computation of MSPC are given in Appendix A of (Benda and Herz, 2003). As the magnitude of  $\Psi_{XY}$ ; MSPC( $\psi_{XY}$ ) reflects the consistency of phase difference over epochs. Like other phase-synchrony measures, MSPC reflects the pure phase relationship between two signals, independently of the signal's amplitude. The value of MSPC varies between 0 and 1, where 1 indicates that the phase relationship is perfectly consistent across epochs, and 0

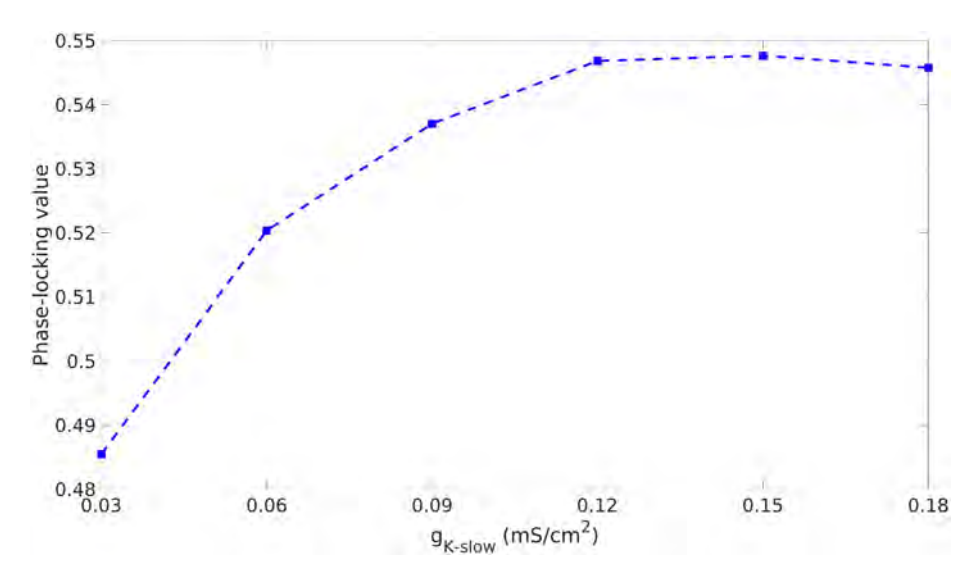


**Fig. 11.** Strength of phase locking between the slow potassium channel activation gate  $(m_{K-slow})$  vs. pooled EPSP. The phase-locking value (PLV) was computed using the multi-spectral phase coherence measure for 1–4 Hz (see Results for details of this measure). With increasing peak slow potassium conductance  $(g_{K-slow})$ , the PLV was found to increase till 0.12 mS/cm<sup>2</sup> beyond which there was saturation.

indicates that the phase relationship is completely random. In our case, both the input and output frequencies are 1–4 Hz and d=1 i.e. we are measuring the *iso*-frequency PLV (see Fig. 11). As in NMC, 16 frequency pairs were included for Bonferroni corrections (1–4 Hz in the input  $\times$  1–4 Hz in the output). With increasing peak slow potassium conductance ( $g_{K-slow}$ ), the PLV was found to increase till 0.12 mS/cm² beyond which there was saturation.

## 4. Discussion

In this study, we examined the effect of a slowly activating outward membrane current, namely the M-type potassium current on the non-linearity in the output of a one-compartment Hodgkin Huxley neuron. The sub-harmonic cross-frequency coupling between the input and output of the neuron was found to increase progressively with an increase in the peak conductance of the slow potassium current while there was no change in the *iso*-frequency coupling. We showed that this slow membrane hyperpolarization mechanism generates low-frequency oscillations, which are not present in the input, due to its slow time scale of operation. Increasing the strength of the peak conductance of the channel associated with this mechanism causes an increase in power in the low frequencies (1–4 Hz) of the membrane voltage. It also increases the low-frequency phase locking between the membrane voltage and the channel activation variable across epochs.

An important question to address is what our results imply in terms of the functional consequences of the observed changes in neurocomputational properties. The ability of spike-frequency adaptation (SFA) to influence information processing depends on both the nature of the input the neuron receives as well as the nature of sampling employed by its downstream targets (Peron and Gabbiani, 2009). SFA has been proposed to be a mechanism of high-pass filtering that preferentially selects for fast stimuli over slow ones (Benda et al., 2005). This has been shown to be particularly important for sensory discrimination. For example, the rapidly adapting electroreceptors in Apteronotus leptorhynchus have a predilection towards fast communication stimuli (Steriade et al., 1993). The frequency selectivity of pyramidal neurons in the cortical map of these electroreceptors has also been shown to be dependent on the expression of slow-potassium channels. However, as our simulation results show, the same slow membrane

mechanisms, when driven by a high frequency input (15–35 Hz), can generate its own low-frequency (1-4 Hz) rhythm (Fig. 8A) that subsequently leaks out into the neuronal activity (Fig. 6). Thus, there is non-linear distortion of the output of the neuron in the form of cross-frequency coupling between the input frequencies to the neuron and these intrinsically generated low frequencies. In fact, previous experimental studies have indeed implicated the role of slow potassium currents in < 1 Hz neo-cortical oscillations (Sanchez-Vives and McCormick, 2000; Steriade et al., 1993). Additionally, cholinergic blockade of these currents have been shown to abolish the slow wave oscillations (Compte et al., 2003). A previous computational study showed how transition to down states mediated by the slowly adapting sodium-dependent potassium current is responsible for generating slow (<1 Hz) neuronal oscillations (Nishino et al., 2011). In line with these evidence, our work provides a quantitative approach to estimating the low-frequency generation mechanism of slow-potassium currents while also showing how the high-pass filtering function of these currents may be distorted by the input-output cross-frequency coupling induced by them.

The role of neuromodulators on slow outward membrane currents can also be insightful in the context of our results. For example, acetylcholine is a central nervous system neuromodulator that is of significant behavioral and functional importance. The level of acetylcholine is elevated during alert, vigilant states and it is associated with a global EEG desynchronization(Steriade, 2004), increased power in higher frequency bands (Bröcher et al., 1992) and increased synaptic plasticity (Aiken et al., 1995). Acetylcholine has also been shown to block slow membrane hyperpolarization and SFA mediated by potassium currents (McCormick, 1993; Gutkin and Ermentrout, 1998). From the dynamical systems point of view, acetylcholine mediated modulation of slow potassium current causes transition between Type 1 and Type 2 excitability (Gutkin et al., 2003; Stiefel et al., 2008). A notable difference between the two firing states is that the firing rate vs. injected current (FI) curve is discontinuous in Type 2 neuron whereas it is continuous in Type 1 neuron. A related difference between the two neuron types is the phase response curve (PRC) where the effect of short depolarizing perturbations given during different phases of the spiking cycle of the neuron is measured when it is being driven by a stable periodic frequency (Roach et al., 2019). While Type 1 neurons show a monophasic response meaning a positive perturbation will uniformly advance a spike generation, Type 2 neurons are biphasic meaning depending on the timing of the perturbation relative to the spiking cycle, the next spike maybe be either advanced or delayed (Koch and Segev, 2000). Such biphasic modulations of the inter-spike intervals can in turn lead to increased cross-frequency input-output coupling (Markram et al., 2003; Yang et al., 2018; Rekling et al., 2000). Our results provide quantitative evidence of how this transition from Type 1 to Type 2 excitability changes the input-output frequency relationship of the neurons. In fact, the reduction in cross-frequency input-output phase coupling is another line of evidence of how high-acetylcholine states may increase the fidelity of rate coding (i.e. iso-frequency coupling).

The monoaminergic neuromodulatory system (serotonin and noradrenaline) has profound and powerful effects on spinal motoneuron excitability which in turn regulate their response to cortical motor commands (Heckman et al., 2009; Sinha et al., 2020). One of the dominant mechanisms of serotonergic raphe system-mediated cranial and spinal motoneuron excitability is the suppression of the calcium-dependent slow potassium current (Sinha et al., 2020). Likewise, at the local spinal circuitry level, cholinergic interneurons promote motoneuron excitability via M2 receptor-mediated reduction in the same slow potassium currents (Miles et al., 2007). Thus, based on the results of our study, increased neuromodulatory drive should reduce the input-output crossfrequency coupling of the motoneurons. However, in our previous study we had also observed a progressive increase in crossfrequency phase coupling between the supraspinal input and the output of the motoneuron pool as the number of interneuron layers increased between them (i.e. as the drive to the motoneurons shifted from the mono-synaptic to the multi-synaptic descending pathways) [71]. These observations open up the avenue of future studies for further exploring the combined effects of mono vs multi-synaptic descending pathways and the neuromodulatory systems (via their effect on the slow potassium currents) on the input-output crossfrequency coupling of spinal motoneurons.

# 5. Limitations and prospects

We acknowledged that there are a few limitations to the current study. First, the range of peak conductances of the slow potassium channel explored in this study was limited by the set of parameters on which the neuron model was based (i.e. cortical interneurons). However, the model is sufficiently minimalistic and does not contain any specializations e.g. dendritic structures, special ion channels, etc. which might affect the generality of the findings. Second, since our study was at the single neuron level, we did not consider the effect of neuronal connectivity at the network level output while varying the strength of the slow conductance mechanism. Thus, the effect of slowly activating outward membrane currents on the emergence of low-frequency oscillations at the neuronal ensemble level can be the prospect of future studies. Thirdly, subtle differences in the mechanisms of different outward membrane currents may affect neuronal encoding differently. For example, a previous study showed that slow outward current mediated by calcium-dependent potassium channels implement noise shaping that improves spike-rate coding of lowfrequency signals, whereas M-type currents implement highpass filtering that improves spike-time coding of high-frequency signals (Aiken et al., 1995). The subtlety lies in the fact that calcium-dependent potassium currents activate in a spikedependent manner while M-currents are spike-independent. Finally, as a logical extension, it will be interesting to compare and contrast the effects of slow membrane hyperpolarization vs.

depolarization mechanisms (like those mediated by persistent inward currents) on the input-output non-linearity of neurons in future studies.

## **Declaration of Competing Interest**

The authors declare that they have no known competing financial interests or personal relationships that could have appeared to influence the work reported in this paper.

# Acknowledgment

The authors would like to thank Dr. Randall K. Powers for carefully revising the manuscript and suggesting valuable edits and corrections. The research leading to these results has received funding supports from the Dixon Translational Research Grants Initiative (Y.Y.) at Northwestern Medicine and Northwestern University Clinical and Translational Sciences Institute (UL1TR001422), NIH R21HD099710 (Y.Y.), R01NS098509 (C.J.H.), R01NS109552 (C.J.H.) and NSF2015317 (C.J.H.).

## **Appendix**

**EPSP** 

$$g_{syn}(t) = g_{max}\left(\frac{t}{t_c}\right)e^{\left(\frac{t-t_c}{t_c}\right)}$$

where  $g_{\text{max}}$  is the peak synaptic conductance and  $t_{\text{c}}$  is the time constant:

$$g_{\text{max}} = 1 \ \text{mS/cm}^2$$

$$t_c = 5 \text{ ms}$$

# **Equilibrium potentials**

$$E_{Na} = 50 \text{ mV}; \ E_K = -90 \text{ mV};$$

$$E_L = -70 \text{ mV}^*$$

\* The leakage equilibrium potential was adjusted to vary the mean firing rate per epoch in the range of 5–50 spikes/s for the same time-varying input (see *Input signal* in *Methods* for details)

**Table 1**Formulation of voltage-dependent ionic channels (Traub et al., 1991; Yamada et al., 1989)

Ion channel	$\begin{aligned} &\text{Activation variable (m)} \\ &(m_{\infty,i} \text{ (V)} = \alpha_{m,i} / (\alpha_{m,i} + \beta_{m,i}) \\ &(\tau_{m,i} \text{ (V)} = 1 / (\alpha_{m,i} + \beta_{m,i})) \end{aligned}$	$\begin{split} &\text{Inactivation variable (h)} \\ &(h_{\infty,i} \text{ (V)} = \alpha_{h,i} /\!\! (\alpha_{h,i} + \beta_{h,i}) \\ &(\tau_{h,i} \text{ (V)} = 1 /\!\! (\alpha_{h,i} + \beta_{h,i})) \end{split}$
Na <sup>+</sup>	$\alpha_{m} = \frac{-0.32(V-VT-13)}{e^{\frac{V-VT-13}{4}}-1}$ $\beta_{m} = \frac{0.28(V-VT-40)}{\frac{V-VT-40}{4}-1}$	$lpha_h = 0.128(e^{-(V-VT-17)/18})$ $eta_h = rac{4}{e^{rac{V-VT-40}{5}}+1}$
$K^+$	$\alpha_{\rm m} = \frac{\frac{-0.032(V-VT-15)}{-0.032(V-VT-15)}}{e^{-\frac{V-VT-15}{5}}-1}$	-
slowK <sup>+</sup> (M-type)	$\begin{split} \beta_{\rm m} &= 0.5 e^{-\frac{(V-V_T-10)}{400}} \\ m_{\infty,K-slow} &= \frac{1}{1+e^{-\frac{(V+35)}{10}}} \\ \tau_{m,K-slow} &= \frac{\tau_{\rm max}}{3.3e^{(V+35)/20} + e^{-(V+35)/20}} \end{split}$	-

<sup>\*</sup>  $\tau_{max}$  = 4 s

 $V_T$  adjusts the spiking threshold, see Table 1 of [35] for the full range of values (for regularly spiking neurons, mean = -61.5  $\pm$  3.2 mV). In our model, we used  $V_T = -60.0$  mV

## Neuron parameters (Pospischil et al., 2008)

 $g_{Na} = 50 \text{ mS cm}^{-2}; g_K = 5 \text{ mS cm}^{-2};$ 

 $g_{K-slow}* = 0.0 - 0.18 \text{ mS cm}^{-2}; g_L = 0.1 \text{ mS cm}^{-2};$ 

\* The  $g_{K-slow}$  parameter was varied in the simulations (see *Simulations* in *Methods* for details)

## Appendix A. Supplementary data

Supplementary data to this article can be found online at https://doi.org/10.1016/j.jtbi.2020.110509.

## References

- Barlow, H.B., 1992. In: "Single Cells versus Neuronal Assemblies," in *Information Processing in the Cortex*. Springer, Berlin Heidelberg, pp. 169–173.
- Sejnowski, T.J., 1995. Time for a new neural code? Nature 376 (6535), 21–22. Fetz, E.E., 1997. Temporal coding in neural populations?. Science 278 (5345), 1901.
- Fetz, E.E., 1997, Temporal coding in neural populations?. Science 2/8 (5345), 1901 https://doi.org/10.1126/science.278.5345.1901.
- B. Nessler, M. Pfeiffer, L. Buesing, and W. Maass, "Bayesian computation emerges in generic cortical microcircuits through spike-timing-dependent plasticity," (in eng), PLoS Comput Biol, vol. 9, no. 4, pp. e1003037-e1003037, 2013, doi: 10.1371/journal.pcbi.1003037.
- Hu, J., Tang, H., Tan, K.C., Li, H., Shi, L., 2013. A spike-timing-based integrated model for pattern recognition. Neural Comput. 25 (2), 450–472.
- Masquelier, T., Hugues, E., Deco, G., Thorpe, S.J., 2009. Oscillations, phase-of-firing coding, and spike timing-dependent plasticity: an efficient learning scheme. J. Neurosci. 29 (43), 13484–13493.
- S. Panzeri, M. E. Diamond, "Information Carried by Population Spike Times in the Whisker Sensory Cortex can be Decoded Without Knowledge of Stimulus Time," (in eng), Front Synaptic Neurosci, vol. 2, pp. 17-17, 2010, doi: 10.3389/ fnsvn.2010.00017.
- Tiesinga, P., Fellous, J.-M., Sejnowski, T.J., 2008. Regulation of spike timing in visual cortical circuits. Nat. Rev. Neurosci. 9 (2), 97–107. https://doi.org/10.1038/pre2215
- Saal, H.P., Wang, X., Bensmaia, S.J., 2016. Importance of spike timing in touch: an analogy with hearing?. Curr. Opin. Neurobiol. 40, 142–149. https://doi.org/10.1016/j.conb.2016.07.013.
- Caporale, N., Dan, Y., 2008. Spike timing-dependent plasticity: a hebbian learning rule. Annu. Rev. Neurosci. 31 (1), 25–46. https://doi.org/10.1146/annurev. neuro.31.060407.125639.
- Enoka, R.M., Duchateau, J., 2017. Rate coding and the control of muscle force. Cold Spring Harb. Perspect. Med. 7 (10), a029702. https://doi.org/10.1101/ cshperspect.a029702.
- Srivastava, K.H., Holmes, C.M., Vellema, M., Pack, A.R., Elemans, C.P.H., Nemenman, I., Sober, S.J., 2017. Motor control by precisely timed spike patterns. PNAS 114 (5), 1171–1176. https://doi.org/10.1073/pnas.1611734114.
- Putney, J., Conn, R., Sponberg, S., 2019. Precise timing is ubiquitous, consistent, and coordinated across a comprehensive, spike-resolved flight motor program. PNAS 116 (52), 26951–26960.
- J. Jeong et al., "Bursting as a source of non-linear determinism in the firing patterns of nigral dopamine neurons," (in eng), Eur. J. Neurosci., vol. 36, no. 9, pp. 3214-3223, 2012, doi: 10.1111/j.1460-9568.2012.08238.x.
- J. Hounsgaard, H. Hultborn, B. Jespersen, and O. Kiehn, "Bistability of alphamotoneurones in the decerebrate cat and in the acute spinal cat after intravenous 5-hydroxytryptophan," (in eng), J Physiol, vol. 405, pp. 345-367, 1988, doi: 10.1113/jphysiol.1988.sp017336.
- Cameron, W.E., Binder, M.D., Botterman, B.R., Reinking, R.M., Stuart, D.G., 1980. Motor unit-muscle spindle interactions in active muscles of decerebrate cats. Neurosci. Lett. 19 (1), 55–60.
- Wei, K., Glaser, J.I., Deng, L., Thompson, C.K., Stevenson, I.H., Wang, Q., Hornby, T.G., Heckman, C.J., Kording, K.P., 2014. Serotonin Affects Movement Gain Control in the Spinal Cord. J. Neurosci. 34 (38), 12690–12700.
- Binder, M.D., Powers, R.K., Heckman, C.J., 2020. Nonlinear input-output functions of motoneurons. Physiology 35 (1), 31–39.
- Stiefel, K.M., Englitz, B., Sejnowski, T.J., 2013. Origin of intrinsic irregular firing in cortical interneurons. Proc. Natl. Acad. Sci. 110 (19), 7886–7891.
- Roberts, J.A., Robinson, P.A., 2012. Quantitative theory of driven nonlinear brain dynamics. NeuroImage 62 (3), 1947–1955. https://doi.org/10.1016/j.neuroimage.2012.05.054.
- McGee, C.G., Haroon, M., Adams, D.E., Luk, Y.W., 2005. A Frequency Domain Technique for Characterizing Nonlinearities in a Tire-Vehicle Suspension System. J. Vib. Acoust. 127 (1), 61–76. https://doi.org/10.1115/1.1855931.
- J. Shils, M. Litt, B. Skolnick, M. Sperling, and M. Stecker, "Bispectral analysis of visual field interactions," in Proceedings of 18th Annual International Conference of

- the IEEE Engineering in Medicine and Biology Society, 31 Oct.-3 Nov. 1996 1996, vol. 3, pp. 974-975 vol.3, doi: 10.1109/IEMBS.1996.652667.
- Victor, J., Shapley, R., 1980. A method of nonlinear analysis in the frequency domain. Biophys. J. 29 (3), 459–483. https://doi.org/10.1016/S0006-3495(80)85146-0.
- Miles, G.B., Hartley, R., Todd, A.J., Brownstone, R.M., 2007. Spinal cholinergic interneurons regulate the excitability of motoneurons during locomotion. Proc. Natl. Acad. Sci. 104 (7), 2448–2453. https://doi.org/10.1073/pnas.0611134104.
- S. B. Laughlin, "The role of sensory adaptation in the retina," Journal of Experimental Biology, vol. 146, no. 1, p. 39, 1989. [Online]. Available: http://jeb.biologists.org/content/146/1/39.abstract.
- Brown, D.A., Adams, P.R., 1980. Muscarinic suppression of a novel voltage-sensitive K+ current in a vertebrate neurone. Nature 283 (5748), 673–676. https://doi.org/10.1038/283673a0.
- Madison, D.V., Nicoll, R.A. "Control of the repetitive discharge of rat CA 1 pyramidal neurones in vitro," (in eng), J Physiol, vol. 354, pp. 319-331, 1984, doi: 10.1113/jphysiol.1984.sp015378.
- Fleidervish, I.A., Friedman, A., Gutnick, M.J. "Slow inactivation of Na+ current and slow cumulative spike adaptation in mouse and guinea-pig neocortical neurones in slices," (in eng), J Physiol, vol. 493 (Pt 1), no. Pt 1, pp. 83-97, 1996, doi: 10.1113/jphysiol.1996.sp021366.
- Bhattacharjee, A., Kaczmarek, L.K. "For K<sup>+</sup> channels, Na<sup>+</sup> is the new Ca<sup>2+</sup>," Trends Neurosci, vol. 28, no. 8, pp. 422-428, 2005, doi: 10.1016/j.tins.2005.06.003.
- F. De Castro, E. Geijo-Barrientos, and R. Gallego, "Calcium-activated chloride current in normal mouse sympathetic ganglion cells," (in eng), J Physiol, vol. 498 (Pt 2), no. Pt 2, pp. 397-408, 1997, doi: 10.1113/jphysiol.1997.sp021866.
- Peron, S.P., Gabbiani, F., 2009. Role of spike-frequency adaptation in shaping neuronal response to dynamic stimuli. Biol. Cybern. 100 (6), 505–520. https://doi.org/10.1007/s00422-009-0304-y.
- Yang, Y., Solis-Escalante, T., van der Helm, F.C.T., Schouten, A.C., 2016. A Generalized Coherence Framework for Detecting and Characterizing Nonlinear Interactions in the Nervous System. IEEE Trans. Biomed. Eng. 63 (12), 2629–2637. https://doi.org/10.1109/TBME.2016.2585097.
- Traub, R.D., Wong, R.K., Miles, R., Michelson, H., 1991. A model of a CA3 hippocampal pyramidal neuron incorporating voltage-clamp data on intrinsic conductances. J. Neurophysiol. 66 (2), 635–650.
- Yamada, W.M., Koch, C., Adams, P.R., 1989. Multiple channels and calcium dynamics. In: Methods in neuronal modeling: From synapses to networks. MIT Press, pp. 97–133.
- Pospischil, M., Toledo-Rodriguez, M., Monier, C., Piwkowska, Z., Bal, T., Frégnac, Y., Markram, H., Destexhe, A., 2008. Minimal Hodgkin–Huxley type models for different classes of cortical and thalamic neurons. Biol. Cybern. 99 (4-5), 427–441. https://doi.org/10.1007/s00422-008-0263-8.
- Pfurtscheller, G., Da Silva, F.L., 1999. Event-related EEG/MEG synchronization and desynchronization: basic principles. Clin. Neurophysiol. 110 (11), 1842–1857.
- Faisal, A.A., Selen, L.P.J., Wolpert, D.M., 2008. Noise in the nervous system. Nat. Rev. Neurosci. 9 (4), 292–303. https://doi.org/10.1038/nrn2258.
- Maltenfort, M.G., Heckman, C.J., Rymer, W.Z., 1998. Decorrelating actions of renshaw interneurons on the firing of spinal motoneurons within a motor nucleus: a simulation study. J. Neurophysiol. 80 (1), 309–323.
- Negro, F., Farina, D., 2011. Decorrelation of cortical inputs and motoneuron output. J. Neurophysiol. 106 (5), 2688–2697.
- Rybak, I.A., Shevtsova, N.A., Lafreniere-Roula, M., McCrea, D.A., 2006/12/01/ 2006,. "Modelling spinal circuitry involved in locomotor pattern generation: insights from deletions during fictive locomotion," (in eng). J. Physiol. 577 (Pt 2), 617–639. https://doi.org/10.1113/jphysiol.2006.118703.
- Rackauckas, C., Nie, Q., 2017. DifferentialEquations.jl A Performant and Feature-Rich Ecosystem for Solving Differential Equations in Julia. Journal of Open Research Software 5, 05/25. https://doi.org/10.5334/jors.151.
- Hagihira, S., Takashina, M., Mori, T., Mashimo, T., Yoshiya, I., 2001. Practical Issues in Bispectral Analysis of Electroencephalographic Signals:. Anesth. Analg. 93 (4), 966–970.
- Dayan, P., Abbott, L.F., 2005. Theoretical Neuroscience: Computational and Mathematical Modeling of Neural Systems. The MIT Press.
- Nikias, C.L., Mendel, J.M., 1993. Signal processing with higher-order spectra. IEEE Signal Process Mag. 10 (3), 10–37.
- Yang, Y., Solis-Escalante, T., van de Ruit, M., van der Helm, F.C.T., Schouten, A.C., 2016. Nonlinear coupling between cortical oscillations and muscle activity during isotonic wrist flexion. Front. Comput. Neurosci. 2016 (10), 126.
- Yang, Y., Schouten, A.C., Solis-Escalante, T., van der Helm, F.C., 2015. Probing the nonlinearity in neural systems using cross-frequency coherence framework. IFAC-papersonline 48 (28), 1386–1390.
- De Hemptinne, C. et al., 2013. Exaggerated phase-amplitude coupling in the primary motor cortex in Parkinson disease. In: Proceedings of the National Academy of Sciences p. 201214546
- Academy of Sciences, p. 201214546.

  Yang, Y., Solis-Escalante, T., Yao, J., Daffertshofer, A., Schouten, A.C., van der Helm, F. C.T., 2016. A General Approach for Quantifying Nonlinear Connectivity in the Nervous System Based on Phase Coupling. Int. J. Neur. Syst. 26 (01), 1550031. https://doi.org/10.1142/S0129065715500318.
- Benda, J., Herz, A.V.M., 2003. A universal model for spike-frequency adaptation. Neural Comput. 15 (11), 2523–2564.
- Benda, J., Longtin, A., Maler, L., 2005. Spike-frequency adaptation separates transient communication signals from background oscillations. J. Neurosc. 25 (9), 2312. https://doi.org/10.1523/JNEUROSCI.4795-04.2005.
- Steriade, M., Nunez, A., Amzica, F., 1993. A novel slow (< 1 Hz) oscillation of neocortical neurons in vivo: depolarizing and hyperpolarizing components. J. Neurosci. 13 (8), 3252–3265.

- Sanchez-Vives, M.V., McCormick, D.A., 2000. Cellular and network mechanisms of rhythmic recurrent activity in neocortex. Nat. Neurosci. 3 (10), 1027–1034. 2000/10/01 2000, doi: 10.1038/79848.
- M. Steriade, F. Amzica, and A. Nuñez, "Cholinergic and noradrenergic modulation of the slow (≈0.3 Hz) oscillation in neocortical cells," J Neurophysiol, vol. 70, pp. 1385-400, 11/01 1993, doi: 10.1152/jn.1993.70.4.1385.
- Compte, A., Sanchez-Vives, M.V., McCormick, D.A., Wang, X.-J., 2003. Cellular and Network Mechanisms of Slow Oscillatory Activity (<1 Hz) and Wave Propagations in a Cortical Network Model. J. Neurophysiol. 89 (5), 2707–2725. https://doi.org/10.1152/jn.00845.2002.
- . "Chapter 47 Hypothalamus, hypocretins/orexin, and vigilance control," in *Handbook of Clinical Neurology* vol. 99, 765–782.
- Steriade, M., 2004. "Acetylcholine systems and rhythmic activities during the waking-sleep cycle," in *Progress in Brain Research* vol. 145:, 179–196.
- Bröcher, S., Artola, A., Singer, W., 1992. Agonists of cholinergic and noradrenergic receptors facilitate synergistically the induction of long-term potentiation in slices of rat visual cortex. Brain Res. 573 (1), 27–36. https://doi.org/10.1016/0006-8993(92)90110-U.
- Aiken, S.P., Lampe, B.J., Murphy, P.A., Brown, B.S., 1995. "Reduction of spike frequency adaptation and blockade of M-current in rat CA1 pyramidal neurones by linopirdine (DuP 996), a neurotransmitter release enhancer," (in eng). Br. J. Pharmacol. 115 (7), 1163–1168. https://doi.org/10.1111/j.1476-5381.1995.tb15019.x.
- McCormick, D.A. "Chapter 36: Actions of acetylcholine in the cerebral cortex and thalamus and implications for function," in Progress in Brain Research, vol. 98, A. C. Cuello Ed.: Elsevier, 1993, pp. 303-308.
- Gutkin, B.S., Ermentrout, G.B., 1998. Dynamics of Membrane Excitability Determine Interspike Interval Variability: A Link Between Spike Generation Mechanisms and Cortical Spike Train Statistics. Neural Comput. 10 (5), 1047–1065.

- Gutkin, B., Pinto, D., Ermentrout, B., 2003. Mathematical neuroscience: from neurons to circuits to systems. Journal of Physiology-Paris 97 (2-3), 209– 219
- K. Stiefel, B. Gutkin, and T. Sejnowski, "Cholinergic Neuromodulation Changes Phase Response Curve Shape and Type in Cortical Pyramidal Neurons," PloS one, vol. 3, p. e3947, 02/01 2008, doi: 10.1371/journal.pone.0003947.
- J. P. Roach, B. Eniwaye, V. Booth, L. M. Sander, and M. R. Zochowski, "Acetylcholine Mediates Dynamic Switching Between Information Coding Schemes in Neuronal Networks," Frontiers in Systems Neuroscience, 10.3389/ fnsys.2019.00064 vol. 13, p. 64, 2019. [Online]. Available: https://www. frontiersin.org/article/10.3389/fnsys.2019.00064.
- Koch, C., Segev, I., 2000. The role of single neurons in information processing. Nat. Neurosci. 3 (S11), 1171–1177.
- Markram, H., 2003. In: Computational Models for Neuroscience. Springer London, London, pp. 125–169. https://doi.org/10.1007/978-1-4471-0085-0\_5.
- Yang, Y., Dewald, J.P.A., van der Helm, F.C.T., Schouten, A.C., . "Unveiling neural coupling within the sensorimotor system: directionality and nonlinearity," (in eng). Eur. J. Neurosci. 48 (7), 2407–2415. https://doi.org/10.1111/ejn.13692.
- Rekling, J.C., Funk, G.D., Bayliss, D.A., Dong, X.-W., Feldman, J.L., 2000. Synaptic Control of Motoneuronal Excitability. Physiol. Rev. 80 (2), 767–852.
- Heckman, C.J., Mottram, C., Quinlan, K., Theiss, R., Schuster, J., 2009. Motoneuron excitability: The importance of neuromodulatory inputs. Clin. Neurophysiol. 120 (12), 2040–2054.
- N. Sinha, J. P. A. Dewald, C. J. Heckman, and Y. Yang, "Cross-Frequency Coupling in Descending Motor Pathways: Theory and Simulation," Frontiers in Systems Neuroscience, 10.3389/fnsys.2019.00086 vol. 13, p. 86, 2020. [Online]. Available: https://www.frontiersin.org/article/10.3389/fnsys.2019.00086.